Experimental Neurology 280 (2016) 106–114

Contents lists available at ScienceDirect

Experimental Neurology

journal homepage: www.elsevier.com/locate/yexnr

Research Paper

RAD001 (everolimus) attenuates experimental autoimmune neuritis by inhibiting the mTOR pathway, elevating Akt activity and polarizing M2 macrophages

Ranran Han [1], Juan Gao [1], Hui Zhai, Jinting Xiao, Ya'nan Ding, Junwei Hao *

Department of Neurology, Tianjin Neurological Institute, Tianjin Medical University General Hospital, Anshan Road, Heping District, Tianjin, 300052, China

ARTICLE INFO

Article history:
Received 21 January 2016
Received in revised form 28 March 2016
Accepted 5 April 2016
Available online 8 April 2016

Keywords:
Experimental autoimmune neuritis
Guillain–Barre' syndrome
Macrophages
mTOR
RAD001

ABSTRACT

Guillain–Barre' syndrome (GBS) is an acute, postinfectious, immune-mediated, demyelinating disease of peripheral nerves and nerve roots. As a classical animal model of GBS, experimental autoimmune neuritis (EAN) has become well-accepted. Additionally, the potent immune modulation exerted by mammalian target of rapamycin (mTOR) inhibitors has been used to treat cancers and showed beneficial effects. Here we demonstrate that the mTOR inhibitor RAD001 (everolimus) protected rats from the symptoms of EAN, as shown by decreased paralysis, diminished inflammatory cell infiltration, reductions in demyelination of peripheral nerves and improved nerve conduction. Furthermore, RAD001 shifted macrophage polarization toward the protective M2 phenotype and modified the inflammatory milieu by downregulating the production of pro-inflammatory cytokines including IFN-γ and IL-17as well as upregulating the release of anti-inflammatory cytokines such as IL-4 and TGF-β. Amounts of the mTOR downstream targets p-P70S6K and p-4E-BP1 in sciatic nerves decreased, whereas the level of its upstream protein p-Akt was elevated. This demonstrated that RAD001 inhibited the mTOR pathway and encouraged the expression of p-Akt, which led to M2 macrophage polarization, thus improved the outcome of EAN in rats. Consequently, RAD001 exhibits strong potential as a therapeutic strategy for ameliorating peripheral poly-neuropathy.

1. Introduction

Guillain–Barre' syndrome (GBS) is an autoimmune disease and an acute inflammatory disorder that afflicts the peripheral nervous system (PNS). GBS is presently the most frequent cause of acute flaccid paralysis worldwide, thereby becoming a leading source of serious neurologic emergencies (Yuki and Hartung, 2012). Proven effective immunotherapies for GBS are plasma exchange and intravenous immunoglobulin G. Nevertheless, despite receiving immunotherapy, approximately 5% of these patients die, and up to 20% suffer from severe disabilities (Hughes et al., 2007). Clearly this affliction is in urgent need of resolution.

Experimental autoimmune neuritis (EAN) has been developed as an animal model of GBS, because it mimics its clinical, histopathological and electrophysiological features. EAN is pathologically characterized by breakdown of the blood-nerve barrier, robust accumulation of reactive T cells and macrophages into the PNS and demyelination of peripheral nerves (Hughes and Cornblath, 2005). During the acute phase, pro-inflammatory cytokines including IL-6, IFN-γ, IL-17 and TNF-α predominate in sciatic nerves and lymphoid organs and mediate inflammatory damage to the peripheral nerves, whereas during the recovery period, anti-inflammatory cytokines such as IL-4 and IL-10 play an essential role in ending the disease course (Zhang et al., 2013; Zhu et al., 1998).

In addition, phenotypically polarized macrophages generally appear either in a pro-inflammatory M1 mode, *i.e.*, classically activated, or in an anti-inflammatory M2, alternatively activated form (Biswas and Mantovani, 2010; Sica and Mantovani, 2012). Such changes of macrophage polarization in the local environment can have a decisive role in the pathogenesis of autoimmune and inflammatory diseases (Jiang et al., 2016; Wynn et al., 2013). IFN-γ has given rise to classically activated macrophages, which secrete IL-1, IL-6 and IL-23. These M1 phenotype macrophages are involved in the induction stage of EAN and are the main contributors to its pathogenic effects and destructive course. As antibody-dependent cellular cytotoxicity and phagocytosis evolve, damage to the myelin sheath may ensue due to the production of reactive oxygen intermediates (Hartung et al., 1988). Meanwhile, alternatively activated M2 macrophages arise mainly in response to IL-4

Abbreviations: GBS, Guillain-Barre' syndrome; EAN, experimental autoimmune neuritis; mTOR, mammalian target of rapamycin; PNS, peripheral nervous system; PBS, phosphate-buffered saline; dpi, days post-immunization; EMG, electromyography; CMAP, compound muscle action potential; MNCV, motor nerve conduction velocity; MNC, mononuclear cell; LFB, luxol fast blue; MTS, 3-(4,5-dimethylthiazol-2-yl)-5-(3-carboxymethoxyphenyl)-2-(4-sulfophenyl)-2H-tetrazolium.

* Corresponding author.
E-mail address: hjw@tmu.edu.cn (J. Hao).

[1] These authors contributed equally to the work.

http://dx.doi.org/10.1016/j.expneurol.2016.04.005

(Mosser and Edwards, 2008). These M2 macrophages contribute to recovery by promoting T-cell apoptosis, secreting anti-inflammatory cytokines like IL-10 and TGF-β (Mantovani et al., 2013) and generating myelin repair and axonal regeneration (Kiefer et al., 2001). A switch of macrophage phenotype from classical activation (M1) to alternative activation (M2) could change the functions of macrophages from inflammatory to anti-inflammatory accompanied by tissue repair (Mosser and Edwards, 2008). Therefore, therapies that facilitate the polarization of macrophages toward the beneficial M2 phenotype may offer protective effects against EAN.

RAD001 (everolimus), an analog of rapamycin, belongs to a group of inhibitors for mammalian target of rapamycin (mTOR), which plays a crucial role in cell proliferation, growth and survival, and mediates its effects mainly by inhibiting mTORC (mTOR complex) 1, with limited or no effect on mTORC2 activity (Saran et al., 2015). Currently, RAD001 is the only mTOR inhibitor approved by the U.S. FDA (Food and Drug Administration) for the treatment of papillary renal carcinoma, pancreatic neuroendocrine tumor, some types of breast cancer and subependymal giant-cell astrocytoma associated with tuberous sclerosis (Agarwala and Case, 2010; Baselga et al., 2012; Curran, 2012; Dorris and Jones, 2014; Yim, 2012). RAD001 has proven effective in reducing those tumors mainly by attenuating the growth of cancer cells under *in vitro* and *in vivo* conditions (Saran et al., 2015). To date, RAD001 has also exerted a protective effect *via* the beneficial regulation of such autoimmune diseases as experimental autoimmune uveoretinitis (Hennig et al., 2012) and autoimmune hepatitis (Ytting and Larsen, 2015). Furthermore, as recently shown, activating the mTOR pathway can downregulate the level of p-Akt, and thus reduce M2 macrophage polarization (Byles et al., 2013). These results prompted our detailed examination of the mTOR pathway and macrophages polarization in treating EAN.

In this study of EAN, we applied RAD001 in preventative and therapeutic patterns and evaluated clinical scores, pathological changes, the distribution of M1/M2 macrophages and inflammatory milieu. As a result, we found that inhibition of the mTOR pathway and activation of Akt attenuated the destructive symptoms of EAN.

2. Materials and methods

2.1. Experimental animals and group assignments

Conditions used here for experiments with rats were approved by the Animal Ethics Committee of the Tianjin Medical University. Lewis rats (male, 160–190 g, 6–8 weeks old) were purchased from the Vital River Corporation (Beijing, China). All rats had access to food and water *ad libitum* and were acclimated to the vivarium environment, which was maintained under temperature-control (23 °C ± 2 °C, 12-h light/dark periods) for one week. Animals were then randomly assigned to one of three groups (preventative, therapeutic or control, $n = 5$ per group). Animal suffering and numbers killed were minimized to the greatest extent possible.

2.2. Induction of EAN and evaluation of clinical signs

To induce EAN, 300 μl of an inoculant containing 300 μg of dissolved P0 peptide 180–199 (10 mg/ml; Bio-Synthesis Corporation) was injected into both hind footpads of each rat. The peptide was dissolved in phosphate-buffered saline (PBS) (2 mg/ml) and then emulsified with an equal volume of complete Freund's adjuvant (CFA; Difco) containing *Mycobacterium tuberculosis* (strain H37RA) to a final concentration of 1 mg/ml. Following immunization, clinical signs of EAN were scored daily in a blinded protocol by two different examiners as follows: 0 = normal; 1 = reduced tonus of the tail; 2 = limp tail; 3 = absent righting reflex; 4 = gait ataxia; 5 = mild paresis of the hind limbs; 6 = moderate paraparesis; 7 = severe paraparesis or paraplegia of the hind limbs; 8 = tetraparesis; 9 = moribund; and 10 = death.

2.3. RAD001 treatment

RAD001 (everolimus) (5 mg/tablet, Novartis) was dissolved in 2 ml ethanol and further diluted in ddWater (endotoxin-free) to a final concentration of 0.2 mg/ml. For preventative treatment, RAD001 solution was administered by oral gavage (1 mg/kg body weight/day) for 16 consecutive days post-immunization (dpi). For therapeutic treatment, the same dose of RAD001 solution was administered by oral gavage daily from the day when the first clinical signs were observed, namely from dpi 7 to 16. Control animals received the same volume of the vehicle solution (*i.e.*, 0.08% ethanol/ddWater). The dosage of RAD001 was based on our previous investigation using different doses (3, 1 and 0.3 mg/kg, daily). The animals treated with 3 mg/kg dose showed higher mortality rate and severe adverse effects: diarrhea, weight loss those were not observed with 1 mg/kg and 0.3 mg/kg daily. And it seemed that 1 mg/kg can exert more significant effect on ameliorating EAN symptoms.

2.4. Electrophysiological studies

Electromyographic (EMG) recordings of the left sciatic nerve in EAN rats were executed on dpi 16 with a fully digital Keypoint Compact EMG/NCS/EP recording system (Dantec Co.). A single blind trial method was applied to record evoked compound muscle action potential (CMAP) amplitudes and latencies of sciatic nerves, as previously described (Sarkey et al., 2007). Rats were anesthetized first with chloral hydrate (intraperitoneally, 3 mg/kg). Two pairs of monopolar needle electrodes were used to stimulate the sciatic nerve and record the signals, respectively. After exposing the left sciatic nerve from the hip (proximal) to the ankle (distal), one pair of needle electrodes was inserted at the sciatic notch (hip/proximal) or the ankle (ankle/distal). The nerve stimulation parameters used to elicit CMAPs were: 1 Hz pulses, with each pulse being 5 mA in amplitude and 0.3 ms in duration. The recording electrodes were positioned in the "belly" part of the gastrocnemius muscle to record evoked potentials from stimulating the sciatic nerve. The motor nerve conduction velocity (MNCV) was calculated by measuring the distance between stimulating cathode electrodes and then measuring the latency difference. The amplitude was calculated from the baseline to the maximal peak under the resulting CMAP curves. After electrophysiologic measurements were completed, the incision was sutured under an aseptic environment. Body temperatures of rats during electrophysiologic measurements were maintained above 34 °C by positioning a heating pad under the rat. For each animal, triplicate measurements were made.

2.5. Histopathological assessment

Following nerve conduction studies, rats were perfused pericardially with cold PBS followed by 4% paraformaldehyde (Solarbio). Then the sciatic nerves were rapidly removed and post-fixed in 4% paraformaldehyde overnight at 4 °C. After dehydration using graded ethanol and vitrification by dimethylbenzene, the nerves were embedded in paraffin (Aladdin). Cross sections 6 μm thick were cut with a microtome (Leica RM2255), mounted on poly-L-lysine-coated slides and stored at room temperature until stained. Hematoxylin-eosin (H&E) (Solarbio) and luxol fast blue (LFB) stains were applied separately to evaluate the extent of inflammatory cell infiltration and demyelination. Results were visualized with a Nikon Coolscope digital microscope. To quantify the inflammatory cell infiltration, 5 fields of each slide were acquired; pictures of each group were collected from 4 different rats. To evaluate the severity of demyelination, histological scores were calculated from fields acquired as described above according to the following semi-quantitative pathological/histological scale: 0, normal perivascular area; 1, mild cellular infiltrate adjacent to the vessel; 2, cellular infiltration plus demyelination in immediate proximity to the vessel; 3, cellular infiltration and demyelination throughout the section. Cell numbers

and histological scores were calculated per square millimeter from each field (200× magnification). All counts were performed in a blinded fashion.

2.6. Lymphocyte proliferation assay

Antigen-specific lymphocyte proliferation was measured by MTS (3-(4, 5-dimethylthiazol-2-yl)-5-(3-carboxymethoxyphenyl)-2-(4-sulfophenyl)-2H-tetrazolium) assays as described previously (Xiao et al., 2014). Briefly, spleens were removed under aseptic conditions and splenocytes were harvested. Single-cell suspensions of splenic mononuclear cells (MNCs) at a density of 2×10^6 cells/ml were allocated with 100 μl culture medium into 96-well microtiter plates. The culture medium was RPMI1640 (containing 2.05 mM glutamine; HyClone) supplemented with 1% (v/v) HEPES buffer solution (Gibco), 0.1% (v/v) 2-mercaptoethanol (Gibco), 1% (v/v) sodium pyruvate (Gibco), 1% (v/v) Pen Strep (Gibco) and 10% (v/v) fetal bovine serum (FBS; Gibco). MNCs were cultured in the presence of either P0 peptide 180–199 (10 μg/ml; Bio-Synthesis Corporation) or without antigen. The concentration of peptide used was based on previous studies (Xiao et al., 2014; Zhang et al., 2014). Following incubation for 72 h at 37 °C and 5% CO_2, MTS solution (Promega) was added, and cells were incubated for an additional 4 h. The absorbance was measured at 490 nm using a microtiter plate reader (Titertek). Since we administered the drug *in vivo*, we could not calculate an inhibitory rate. The data are presented as mean OD ± SEM. The experiment was performed with MNCs from four different rats in each group, and MNCs from each rat were done in triplicate.

2.7. Fluorescence immunohistochemistry

Following nerve conduction studies, the sciatic nerves were harvested as described above and post-fixed in 4% paraformaldehyde overnight at 4 °C. The nerves were dehydrated sequentially in 15% and then 30% sucrose until equilibrated. Afterward, nerves were embedded in Tissue-tek medium (SAKURA) and snap-frozen in liquid nitrogen to expose antigenic sites for staining. Transverse slices (8 μm) were made on a cryostat (Leica Microsystems LM3050S) and then mounted on poly-L-lysine-coated slides and stored at −80 °C.

Fluorescence immunohistochemistry for the frozen specimens was performed using standard protocols provided by the antibody manufacturers. Briefly, after a 20 min interval to reach room temperature, the slides were fixed and blocked for half an hour at 37 °C with 3% BSA in PBS with 0.3% Triton X-100. The mounted tissue was then incubated overnight at 4 °C with primary antibodies: mouse anti-CD68 (1:200, Abcam); rabbit anti-CD86 (1:200, Abcam) and goat anti-CD206 (1:200, Santa Cruz Biotechnology) diluted in the same blocking solution. On the next day, the slides were washed in cold PBS and incubated for 1 h at room temperature with the following species-appropriate fluorochrome-conjugated secondary antibodies: Rhodamine (TRITC) AffiniPure donkey anti-goat IgG (H + L) (1:100, Jackson Immunoresearch); Rhodamine (TRITC) AffiniPure donkey anti-rabbit IgG (H + L) (1:100, Jackson Immunoresearch) and Alexa Fluor® 488 conjugated donkey anti-mouse IgG (H + L) (1:1000, Thermo Fisher Scientific). After five more washes, the tissue was coverslipped with fluoroshield mounting medium containing DAPI (Abcam) to counterstain cell nuclei. Immunostaining was visualized with a Coolscope (Nikon). Positive cell numbers were calculated per square millimeter from three random microscopic fields (200× magnification). All counts were performed in a blinded fashion.

2.8. Flow cytometry

Spleens were removed under aseptic conditions on dpi 16, and splenocytes were harvested after lysing red blood cells. 1×10^6 spleen MNCs resuspended in 100 μl PBS/1% BSA were co-stained for cell surface CD11b conjugated with phycoerythrin (1:100, Abcam); MHCIIa marker for M1 macrophages, was conjugated with APC (1:100, Abcam) and/or CD206 (1:100, Abcam), a specific marker for M2 macrophages for 45 min at room temperature following the manufacturer's specifications. After washing, Alexa Fluor®647-labelled donkey anti-rabbit IgG (H&L) secondary antibody (1:1000, Abcam was applied for CD206. MNCs were gated by forward and sideways scatter. Surface molecule expression was evaluated by detecting the percentage of positive cells. Cells from all groups were collected and analyzed at each time-point on the same day with the same cytometer settings. Flow cytometric data were acquired using a FACSAria™ flow cytometer (BD Biosciences) and analyzed with FlowJo software version 7.6.1 (flowjo.com).

2.9. Western blot analysis

Total protein was obtained from sciatic nerves stored in liquid nitrogen by applying Trizol (Ambion) as the manufacturer instructed. Samples adjusted to equal content and volume were loaded on 12% SDS-PAGE gels and electrophoretically separated. Then proteins were transferred to PVDF membranes (Millipore). Membranes were blocked in 5% BSA dissolved in Tris-buffered saline solution for 1 h, followed by overnight primary antibody incubation at 4 °C. The following antibodies were used: p-4E-BP1, p-P70S6K, p-Akt, all diluted 1:1000 (Cell Signaling Technology) and actin (1:2000, Zhongshanjinqiao). On the next day, membranes were washed then, incubated with goat anti-rabbit IgG or goat anti-mouse IgG conjugated to horseradish peroxidase at a 1:5000 dilution (Transgen Biotech) at room temperature for 1 h. The protein-specific signals were detected using a Bio-Rad 721BR08844 Gel Doc Imager (Bio-Rad) and expressed as a fraction of corresponding β-actin.

2.10. ELISA for cytokine profile

The supernatants of splenic MNCs (2×10^6 cells/ml) cultured with or without P0 peptide 180–199 (10 μg/ml) were collected after incubation for 72 h at 37 °C with 5% CO_2. Simultaneous quantitative analysis of twelve cytokines, including IL-1α, IL-1β, IL-2, IL-4, IL-6, IL-10, IL-12, IL-13, IFN-γ, TNF-α, GM-CSF and RANTES was performed using a multi-analyte ELISArray Kit (QIAGEN) according to the manufacturer's instructions. Determinations were performed in triplicate, and results are expressed as mean OD ± SEM ($n = 4$).

2.11. Real-time (RT) quantitative PCR

Total RNA was isolated from splenic cells with Trizol reagent (Ambion) according to the manufacturer's instructions on dpi 16. The first strand of cDNA was synthesized from 10 μg of RNA with TransScript First-Strand cDNA Synthesis SuperMix (Transgen Biotech). RT-PCR was performed on the Opticon 2 Real-Time PCR Detection System (Bio-Rad) and SYBR green PCR MasterMix (Roche) using the primers as displayed in Table 1. Samples were run in duplicate at 95 °C for 10 min, then 40 cycles at 95 °C for 15 s, and finally at 60 °C for 1 min. The results were analyzed automatically by an ABI SteponePlus instrument, and the

Table 1
Primers sequences for real-time quantitative RT-PCR.

Genes	Primers (forward and reverse)
IFN-γ	5′-TCGCACCTGATCACTAACTTCTTC-3′
	5′-CGACTCCTTTTCCGCTTCC-3′
IL-4	5′-TGATGGGTCTCAGCCCCCACCTTGC-3′
	5′-CTTTCAGTGTTGTGAGCGTGGACTC-3′
IL-17	5′-TGGACTCTGAGCCGCATTGA-3′
	5′-GACGCATGGCGGACAATAGA-3′
TGF-β	5′-CTTCAGCTCCACAGAGAACTGC-3′
	5′-CACGATCATGTTGGACAACTGCTCC-3′
β-actin	5′-CCGTCTTCCCCTCCATCGT-3′
	5′-ATCGTCCCAGTTGGTTACAATGC-3′

method of $2^{-\Delta\Delta Ct}$ was used to analyze mRNA expression. Expression levels of the mRNAs were then reported as fold changes vs control. Results are expressed as mean OD ± SEM ($n = 3$–5).

2.12. Evaluation and statistical analysis

The Mann-Whitney *U* test was used to compare differences between the control group and treatment groups where appropriate (GraphPad Prism 5.0). Data are presented as means ± SEM. For all statistical analyses, the level of significance was set at $p < 0.05$.

3. Results

3.1. RAD001 treatment ameliorates symptoms, improves histological changes and reduces inflammatory cell accumulation in EAN rats

RAD001 was applied in two different paradigms tor treating EAN rats (Fig. 1). For the preventative pattern (blue line), we administered RAD001 (1 mg/kg/day) by gavage after immunization to the peak phase (dpi 16). Alternatively, for the therapeutic pattern (green line), the same dose of RAD001 was applied only after the first clinical symptoms of the disease appeared. In both RAD001-treated groups, the scores for severity of EAN decreased; that is, compared to rats in the control group, the preventative treatment group manifested significant better clinical scores from day 7 to day 16 ($p < 0.05$ on each time point). However, the statistically significant difference occurred 10 to 16 dpi ($p < 0.05$ on each time point) between the therapeutic treatment group and the control group. The mean peak clinical scores were 3.20 ± 0.58, 3.50 ± 0.22, and 6.90 ± 0.29 in the preventative, therapeutic, and control groups, respectively (Fig. 1A and B). Notably, in the preventative treatment group, the first clinical sign of impairment was delayed until day 9.20 ± 0.20 (Fig. 1A and C), whereas such signs appeared sooner in the therapeutic group at 7.20 ± 0.20 dpi and in the control group at 6.80 ± 0.20 dpi (Fig. 1C).

We assessed the histopathology of EAN rats' sciatic nerves at the peak phase of the clinical course (*i.e.*, 16 dpi). H&E staining was used to exhibit inflammatory cell infiltration, and LFB staining was applied to reveal demyelination. Treating EAN rats with RAD001 in both paradigms (*i.e.*, preventative and therapeutic) not only lowered the counts

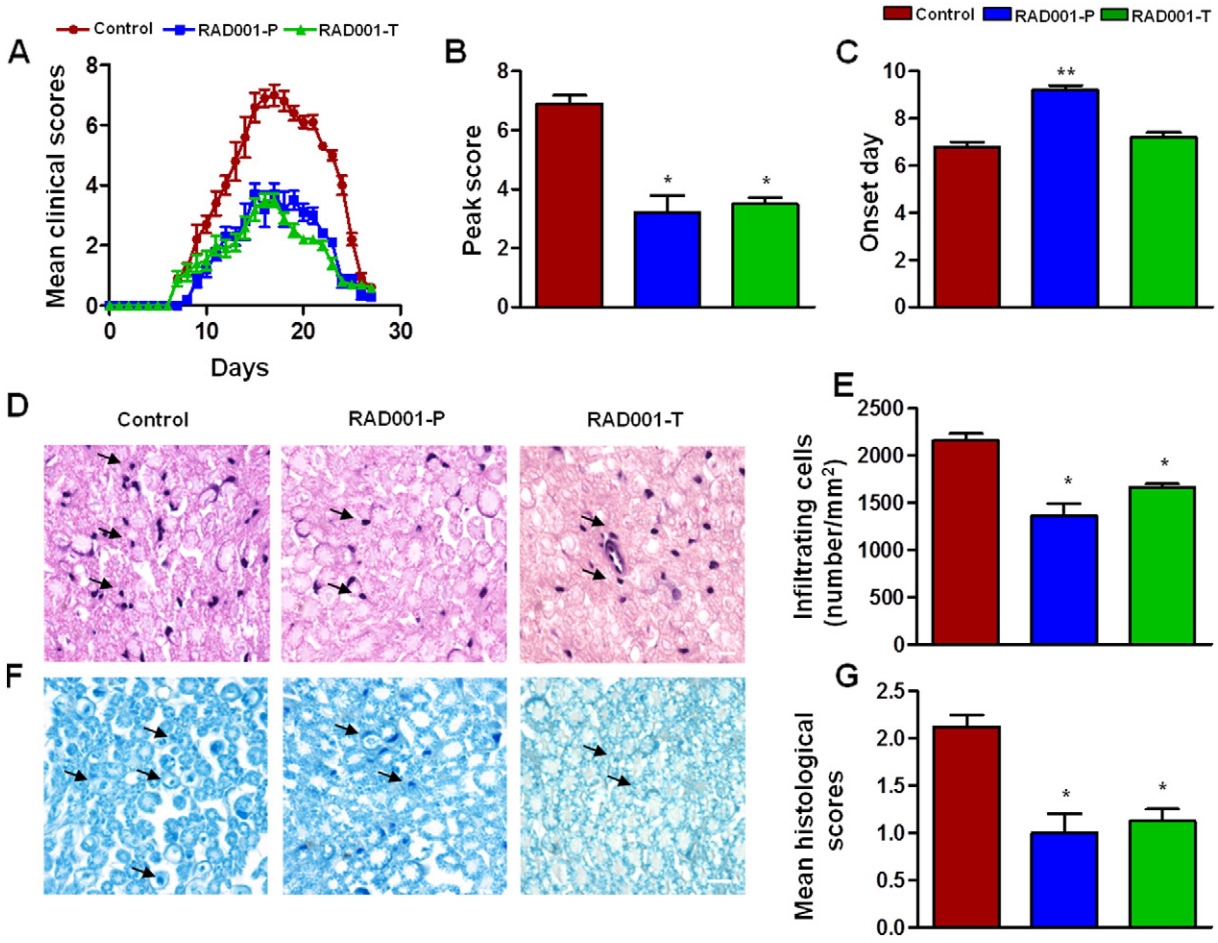

Fig. 1. RAD001 treatment ameliorates the severity of EAN. In a preventative treatment paradigm, RAD001 was administered from day 1 to day 16 (1 mg/kg, once daily) to EAN rats. The same dosage was applied in a therapeutic treatment paradigm from day 7 to day 16. As a control condition, EAN rats received an equivalent volume of vehicle. Clinical scores (0–10, with 0 being normal to 10 being so severely impaired that the animals died) were assessed daily post-immunization (dpi). (A) EAN clinical scores were markedly better in RAD001-treated groups, but the pattern of improvement over time was uneven. The rats in the preventative and therapeutic group displayed notably better clinical scores from day 7 to day 16 and from day 10 to day 16 (each group compared separately) with the control group ($p < 0.05$ on each time point). (B—C) RAD001 improved the peak score and delayed the day of disease onset in EAN rats. On dpi 16, sciatic nerves of EAN rats were recovered for H&E staining (D) and LFB staining (F) to assess changes in inflammatory cell infiltration and demyelination. Representative photomicrographs are shown for each group. Arrows in D show the inflammatory cells and in F show the demyelination and inflammatory cell. The mean number of inflammatory cells per mm^2 tissue section was evaluated as described in Materials and Methods, and summaries are shown in (E). Mean histological scores are shown in (G). Scores were calculated as described in Materials and Methods. Comparisons between the control group and RAD001-treated groups were performed using Mann-Whitney *U* tests. Scale bar in D and F is 10 μm. The results are presented as means ± SEM (*$p < 0.05$ **$p < 0.01$ for comparison between control and RAD001-treated groups, $n = 5$ per group for clinical scores and $n = 4$ per group for staining). The experiment was repeated 2 times with similar results. RAD001-P, preventative RAD001 group; RAD001-T, therapeutic RAD001 group.

of inflammatory cells (Fig. 1D and E) but also reduced the degree of demyelination and inflammatory cell infiltration (Fig. 1F and G).

3.2. RAD001 alleviates EAN-induced peripheral nerve injury

As is well known, EAN-induced peripheral nerve injury can decrease CMAP amplitude and MNCV as well as lengthening CMAP latency. Therefore, we estimated the ability of RAD001 to improve this situation by evoked response electrophysiology at dpi 16 in the sciatic nerve and gastrocnemius muscle. In accordance with the clinical findings shown in Fig. 1, RAD001 alleviated the severity of peripheral nerve deficits in both RAD001-treated groups (Fig. 2). For the MNCV, the control group's mean speeds were slower than the preventative and therapeutic groups' speeds (33.3 ± 1.2 m/s *vs.* 52.6 ± 3.5 m/s and 46.3 ± 1.2 m/s, $p < 0.05$, Fig. 2C). The CMAP mean amplitudes of the two RAD001-treatment groups were greater (13.4 ± 2.2 mV and 17.3 ± 2.0 mV, respectively, Fig. 2D) compared to those of the control group (7.4 ± 0.6 mV). Also, CMAP latency was shorter in the preventative group and therapeutic group, showing beneficial effects of RAD001 compared to the control group's average latency ($p < 0.05$, Fig. 2E).

3.3. RAD001 ameliorates lymphocyte proliferative responses

MNCs isolated from EAN rat spleens at the peak phase of disease (dpi 16) were stimulated *in vitro* with P0 peptide 180–199 (10 μg/ml) or without peptide for 72 h to assess the effect of RAD001 on lymphocyte proliferative responses (Fig. 3). Compared to the control group, the RAD001 recipients in preventative and therapeutic groups showed significantly lower levels of lymphocyte proliferation (2.35 ± 0.34 *vs.* 0.98 ± 0.16, and 0.73 ± 0.18, respectively) with P0 peptide stimulation (Fig. 3A, $p < 0.05$) and the same trend without peptide stimulation (1.89 ± 0.29 *vs.* 0.88 ± 0.12, and 0.67 ± 0.14, respectively), as evaluated by MTS assay.

3.4. RAD001 promotes M2 macrophage polarization in EAN rats

Double-immunohistochemical staining with the macrophage marker CD68 and either CD86, a marker for the M1 phenotype, or CD206, a marker for the M2 phenotype, was used to identify the proportion of

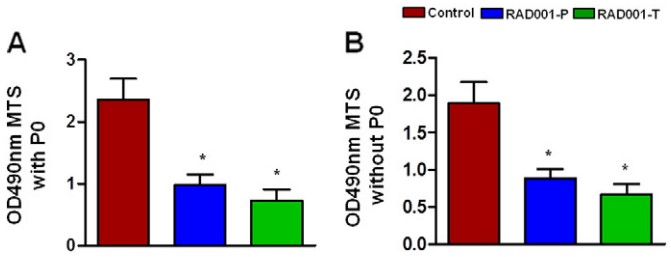

Fig. 3. RAD001 alleviates MNC proliferation Splenic mononuclear cells (MNCs) from each group were evaluated on dpi 16. After culturing for 72 h in the presence or absence of P0 peptide 180–199 (10 μg/ml), MNC proliferation was analyzed by MTS assay. When compared to the control group, the RAD001-treatment groups underwent significant reductions in proliferation with (A) or without (B) P0 peptide stimulation. Each experiment was performed in triplicate for each group. The control group and RAD001-treated groups were compared by Mann-Whitney *U* tests. Data shown are means ± SEM (*$p < 0.05$ for comparison between control and RAD001-treated groups, $n = 4$ per group). The experiment was repeated 2 times with similar results. RAD001-P, preventative RAD001 treatment; RAD001-T, therapeutic RAD001 treatment.

M1 and M2 cells in sciatic nerves. The polarization state of MNCs derived from spleens of rats given RAD001 for treatment or prevention of EAN was investigated *via* flow cytometry. In sciatic nerves harvested on dpi 16, RAD001-preventative and RAD001-therapeutic groups both displayed elevated local expression of M2 macrophages and reduced expression of M1 macrophages compared to the control group (Fig. 4A–C, $p < 0.05$). Flow cytometric results indicated an elevation of M2 expression in spleen MNCs. Additionally, both the RAD001-preventative and RAD001-therapeutic groups showed elevated expression of M2 macrophages in EAN spleens compared to the control group (Fig. 4D–E, $p < 0.05$).

3.5. RAD001 inhibits p-P70S6K and p-4E-BP1 yet increases p-Akt protein levels in sciatic nerves of EAN rats

The 4E-BP1 and P70S6K proteins are two main downstream products of the mTOR signaling pathway, and this pathway is regulated by the level of Akt. Since RAD001 is a potent inhibitor of the mTOR pathway, we explored the extent of 4E-BP1, P70S6K and Akt activity in sciatic nerves taken from EAN rats on dpi 16. According to Western blotting

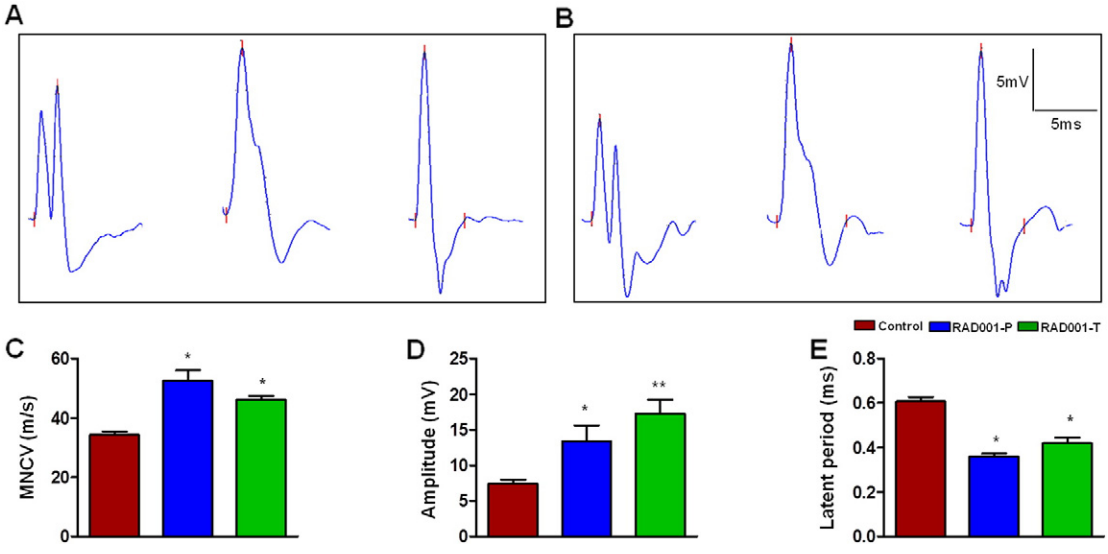

Fig. 2. RAD001 improves peripheral nerve conduction deficits in EAN rats. Representative electrophysiological recordings of motor nerve compound muscle action potentials (CMAPs) evoked from stimulation of the fibular head (A) or ankle regions (B) of the sciatic nerve are shown for control, RAD001-P, and RAD001-T rats, respectively, from left to right. Compared to the control group, RAD001-treated groups were protected from EAN-induced damage of mean motor nerve conduction velocity (MNCV) (C). RAD001-treated groups had improved amplitudes of CMAPs (D) and also exhibited better distal motor latencies of CMAPs (E) when compared to the control group. The control group and RAD001-treated groups were compared by Mann-Whitney *U* testing. Data shown are the means ± SEM (*$p < 0.05$, for comparison between control and RAD001-treated groups; $n = 4$ per group). The experiment was repeated 2 times with similar results. RAD001-P, preventative RAD001 group; RAD001-T, therapeutic RAD001 group.

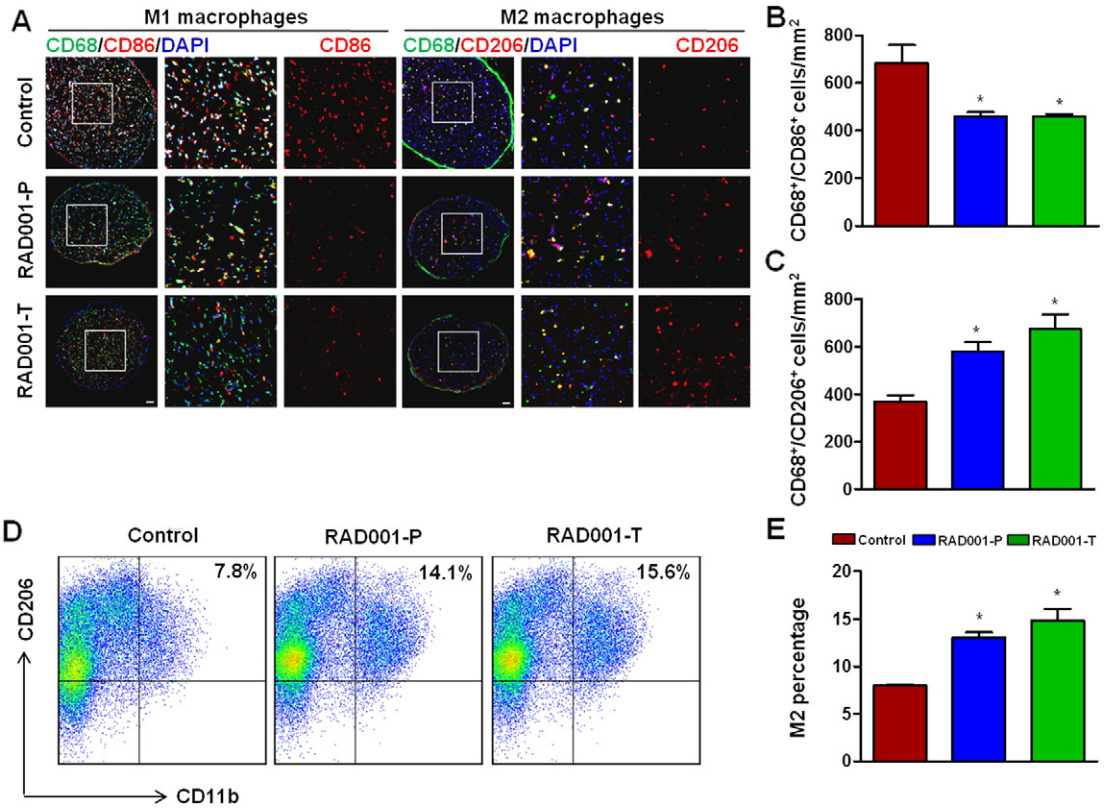

Fig. 4. RAD001 promotes M2 macrophage polarization in EAN At the peak phase of EAN after RAD001 treatment, each rat's sciatic nerves were harvested for fluorescent immunohistochemistry, and spleen mononuclear cells (MNCs) were isolated for flow cytometry, in both cases to analyze the percentage of M1 and M2 macrophages (A) Fluorescence photomicrographs showed M1 and M2 macrophages in the sciatic nerves of EAN rats. Tissue sections were stained for markers of M1 and M2 macrophages as indicated. Scale bar is 100 μm. (B) Quantitation of immunofluorescence. Counts per mm^2 of $CD68^+/CD86^+$ cells (M1 phenotype) in sciatic nerves showed that RAD001 reduced the number of M1 macrophages in both RAD001 treatment paradigms. (C) Counts per mm^2 of $CD68^+/CD206^+$ cells (M2 phenotype) showed that both RAD001-treated groups had increased numbers of M2 macrophages compared to controls. (D) Flow cytometry of spleen MNCs in EAN rats. (E) Quantitation of flow cytometry. Percentage of M2 macrophages in spleen MNCs was greater in both RAD001-treated groups compared to the control group. Comparisons to control group were performed using the Mann-Whitney *U* test; quantitation shows means ± SEM ($^*p < 0.05$ for comparison between control and RAD001-treated groups; $n = 4$ per group). The experiment was repeated 2 times with similar results. RAD001-P, preventative RAD001 treatment; RAD001-T, therapeutic RAD001 treatment.

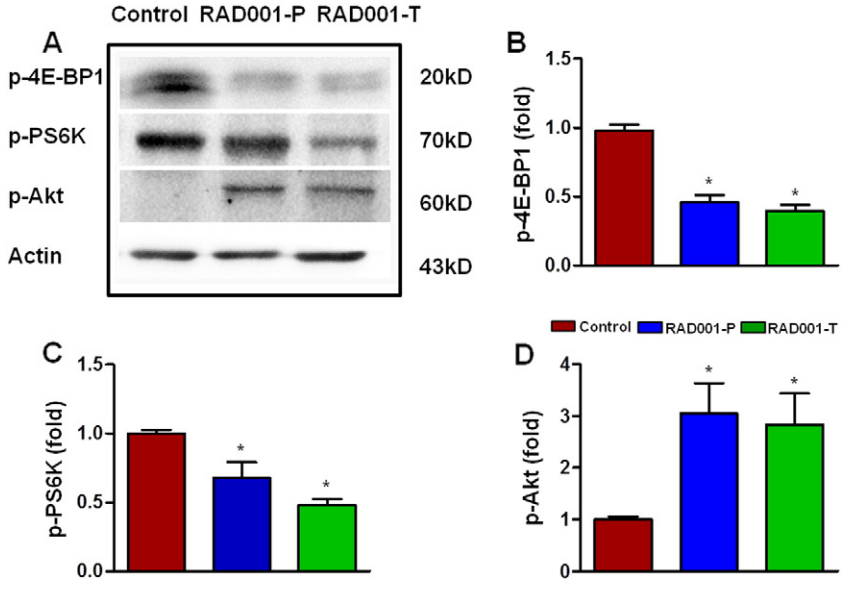

Fig. 5. RAD001 treatment inhibits the production of p-4E-BP1 and p-P70S6K, but increases the level of p-Akt in sciatic nerves of EAN rats On dpi 16, sciatic nerves of each rat were harvested for Western blotting. (A) Western blots of p-4E-BP1, p-P70S6K and p-Akt protein compared to a β-actin standard. RAD001-preventative and RAD001-therapeutic groups had decreased expression of p-4E-BP1 and p-P70S6K and an increased level of p-Akt in sciatic nerves when compared to the control group. (B–D) Quantitation of Western blots of p-4E-BP1, p-P70S6K and p-Akt. Relative expression of p-4E-BP1 and p-P70S6K in RAD001-treated groups was significantly greater compared to the control group, whereas the level of p-Akt was reversed. Comparisons to control group were performed using the Mann-Whitney *U* test; quantitation shows means ± SEM ($^*p < 0.05$ for comparison between control and RAD001-treated groups; $n = 3$–4 per group). The experiment was repeated 2 times with similar results. RAD001-P, preventative RAD001 treatment; RAD001-T, therapeutic RAD001 treatment.

analysis, RAD001-preventative and RAD001-therapeutic groups evinced robust localized cellular expression of p-Akt but inhibition of p-4E-BP1 and p-P70S6K compared to the control group (Fig. 5A–D, $p < 0.05$).

3.6. RAD001 alters cytokine profile

As is well documented, the expression profiles of cytokines affect the outcome of EAN. We confirmed relevant changes in cytokine production in RAD001-treated splenic MNCs by using RT-PCR. That is, IFN-γ and IL-17 mRNA levels were greatly reduced in RAD001-treated groups compared to those in the control group, whereas TGF-β and IL-4 mRNA levels increased significantly (Fig. 6A–D, $p < 0.05$). Semi-quantitative analysis followed to assess the effects of RAD001 treatment on the cytokine profiles produced *in vitro* by MNCs from EAN rats in response to the presence or absence of P0 peptide 180–199 (10 μg/ml). Results from using multi-cytokine ELISA kits showed that, the production of pro-inflammatory cytokines (IL-1α, IFN-γ and RANTES) by MNCs was reduced significantly in both RAD001-treatment groups compared to that in the control group (Fig. 6E). By contrast, levels of the anti-inflammatory cytokine IL-10 were upregulated. However, no marked differences were recorded for the amounts of IL-1β, IL-2, IL-4, IL-6, IL-12, IL-13, TNF-α or GM-CSF among the three groups. Besides, the differences between the three groups without antigen stimulation were meaningless (data not shown).

4. Discussion

In this study, we used a classic animal model of GBS, *i.e.*, EAN, to quantify the effect of RAD001 for treating and/or preventing this disease. As a result, RAD001 significantly ameliorated the symptoms of EAN rats, documented here by the milder inflammatory responses, lesser demyelination of peripheral nerves and improved nerve conduction in RAD001-treated groups. Additionally, RAD001 increased the percentage of M2 macrophage polarization, as demonstrably related to inhibition of the mTOR signaling pathway and heightened activation of Akt.

Assessing neurological symptoms through clinical scores, we observed that RAD001 greatly diminished EAN symptoms by reducing the severity of paralysis, delaying the onset of EAN and decreasing the peak clinical score. Further, RAD001 generally protected nerves from EAN-induced peripheral nerve injury by improving MNCV and amplitudes of CMAPs and by reducing the distal motor latency compared to those values in controls. Histopathologically, EAN is characterized by inflammatory cell infiltration and nerve demyelination. In the present study, both preventative and therapeutic RAD001 administration significantly suppressed the accumulation of inflammatory cells and deterred demyelination when compared to those qualities in the control group.

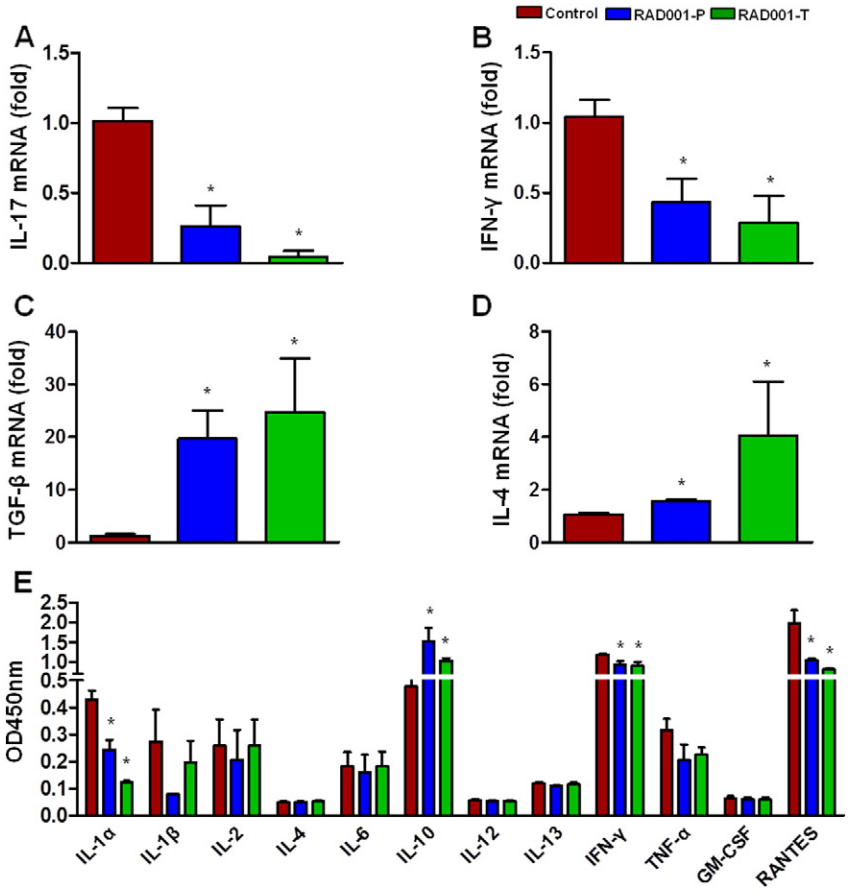

Fig. 6. RAD001 alters cytokine profiles Splenic mononuclear cells (MNCs) from each rat were harvested on dpi 16. (A–D) mRNA levels of inflammatory cytokines in the MNCs from EAN rats. Levels of the pro-inflammatory cytokines IFN-γ and IL-17 decreased in RAD001-treated groups, but those of the anti-inflammatory cytokines TGF-β and IL-4 increased significantly. (E) Cytokine profiles of the supernatants of splenic MNCs cultured with P0 peptide 180–199 (10 μg/ml) for 72 h, as measured by ELISA. Levels of IL-1α, IFN-γ and RANTES decreased greatly, but the level of IL-10 increased compared to the control group. No marked differences appeared for the levels of IL-1β, IL-2, IL-4, IL-6, IL-12, IL-13 TNF-α and GM-CSF among the three groups. Each experiment was performed in triplicate for each group. The control group and RAD001-treated groups were compared using Mann-Whitney *U* tests. Data shown are means ± SEM (*$p < 0.05$ for comparison between control and RAD001-treated groups, $n = 3$–5 per group). The experiment was repeated 2 times with similar results. RAD001-P, preventative RAD001 treatment; RAD001-T, therapeutic RAD001 treatment.

Overall, these results demonstrated the marked beneficial effects of RAD001 on EAN rats.

Macrophages are generally divided into two types: classically activated (M1) and alternatively activated (M2) macrophages (Gordon, 2003). M1-type macrophages release cytokines that inhibit the proliferation of surrounding cells and damage contiguous tissue, whereas M2-type macrophages release cytokines that promote the proliferation of contiguous cells and repair tissue (Mantovani et al., 2013). Furthermore, alternatively activated M2 macrophages play an immunomodulatory role in EAN (Zhang et al., 2012; Zhang et al., 2009), leading to a favorable outcome. In agreement with those findings, the present study showed that the improved outcome of EAN rats was associated with the differentiation of macrophages toward the M2 phenotype. That is, the sciatic nerves of RAD001-treated EAN rats clearly contained more M2-type and fewer M1-type macrophages. In addition, flow cytometry results confirmed that splenic macrophages in RAD001-treated EAN rats polarized more toward the M2 type. This combined evidence supported the opinion that RAD001 improved the prognosis of EAN by promoting M2 type polarization.

The well-known mTORC1-mediated feedback inhibition of Akt signaling (Byles et al., 2013; Carracedo et al., 2008; Song et al., 2012) is reinforced by our findings that inhibiting the mTOR signaling pathway *via* lowering expression of its target products p-4E-BP1 and p-P70S6K promoted activation of p-Akt (Fig. 7). Although other negative feedback mechanisms have been described (Shi et al., 2005; Song et al., 2012), and may exist in our setting, they act synergistically and ultimately converge to promote Akt activation (O'Reilly et al., 2006). In addition, we believe that feedback activation of Akt can underlie the enhanced polarization of M2 macrophages (Fig. 7). Vanessa Byles et al. reported that downregulation of Akt, which may be a response to elevated mTORC1 activation, could impair the activation of M2 macrophages (Byles et al., 2013). They also asserted that treatment of rapamycin, an mTOR inhibitor, *in vivo* modestly increased Akt signaling and M2 responses (Byles et al., 2013). Guohua Wang et al. proposed that activation of Akt *in vivo* can promote M2 microglia/macrophage polarization, which in turn may lead to an anti-inflammatory effect (Wang et al., 2015). To the contrary, Mercalli et al. embraced a conflicting conclusion after using rapamycin for 3 weeks and finding an unbalanced diversion of macrophages to the M1 phenotype (Mercalli et al., 2013). Su et al attributed the conflicting conclusions to a context dependence of mTORC1 function in innate immunity (Su et al., 2015). In this work we demonstrated that the activation of Akt can partly underlie the polarization of M2 macrophages in EAN rats. The underlying mechanisms for such differences are unknown, probably due to stimulus- and context-specific regulatory mechanisms during macrophage polarization. Although our results strongly indicated that RAD001 modulated macrophage phenotype switching in EAN, previous study has reported that macrophage polarization induced by mTOR inhibitor rapamycin was at least partially due to interaction of macrophages and regulatory T cells (Xie et al., 2014). In addition, macrophage phenotype switch been accompanied by inhibition of Th1 and Th17 cells and activation of Th2 and regulatory T cell can favor the outcome of EAN (Zhang et al., 2009). Therefore, the possibility that cell types other than macrophages mediate RAD001-induced protective effects (Chi, 2012; Saran et al., 2015; Xie et al., 2014), especially in EAN, warrants further studies.

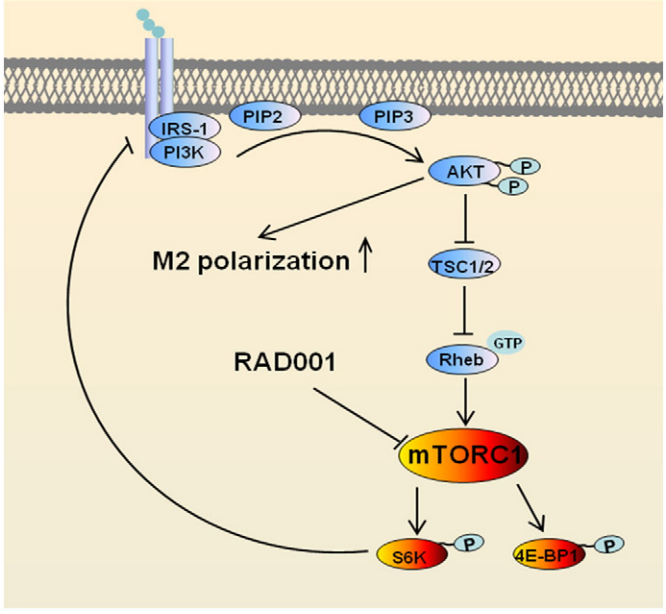

Fig. 7. Proposed mechanism underlying the effect of RAD001 on macrophage polarization RAD001 inhibited mTORC1 thereby decreasing the activity of p-P70S6K and p-4E-BP1. Downregulated p-P70S6K then lost the feedback loop, leading to an increased activation of phosphatidyl inositol 3-kinase (PI3K). Active PI3K converts phosphatidyl (4,5)-biphosphate (PIP2) to phosphatidylinositol (3,5)-triphosphate (PIP3), thereby activating the prosurvival kinase Akt. Activated Akt can then shift macrophages from the destructive M1 phenotype toward the beneficial M2 phenotype thus eliciting the protection of peripheral nerves. Rheb, Ras homolog enriched in brain. IRS-1, insulin receptor substrate 1.

RAD001 was verified as means of ameliorating inflammatory responses in animal models of experimental autoimmune uveoretinitis (Hennig et al., 2012), autoimmune hepatitis (Ytting and Larsen, 2015) and in healthy volunteers(Vitiello et al., 2015) as well as in renal transplant recipients (Pereira-Lopes et al., 2013). In accordance with previous reports, the present study showed that RAD001 reduced inflammatory responses in EAN rats and favored successful outcomes. RAD001 reduced the mRNA expression of IFN-γ and IL-17, and upregulated the mRNA expression of IL-4 and TGF-β in the spleens of EAN rats. In addition, the same trend of decreased pro-inflammation and increased anti-inflammation cytokine profiles were observed in ELISA analyses of supernatants from cultured splenic MNCs. These data revealed that RAD001's ability to deter destruction by the inflammatory environment was a basis for the protective effect in EAN. Although the spleen samples used here were taken from animals given RAD001 *in vivo*, therefore may not duplicate changes in peripheral nerves *in situ*, our data nonetheless provided mechanistic insight into the physiological activities underpinning this potentially valuable therapeutic strategy. Therefore, the positive clinical outcome we observed sheds light on a likely solution to a heretofore inevitable course of disease.

5. Conclusions

We have demonstrated that RAD001 attenuated EAN through an Akt-mediated phenotypic shift in macrophages. The anti-inflammatory effects of RAD001 in EAN, and possibly its human counterpart, GBS, may improve the environmental milieu and indirectly exert neuroprotective effects. RAD001 thus can be a potent candidate for alleviating polyneuritic disease.

Disclosure

All authors report no conflict of interest.

Acknowledgement

This work was financially supported by the National Natural Science Foundation of China (81322018, 81273287, and 81100887 to J.W.H.); the Program for New Century Excellent Talents in University of China (NCET 111067 to J.W.H.); and the Key Project of Natural Science Foundation of Tianjin Province (12JCZDJC24200 to J.W.H.).

References

Agarwala, S.S., Case, S., 2010. Everolimus (RAD001) in the treatment of advanced renal cell carcinoma: a review. Oncologist 15, 236–245.

Baselga, J., Campone, M., Piccart, M., Burris 3rd, H.A., Rugo, H.S., Sahmoud, T., Noguchi, S., Gnant, M., Pritchard, K.I., Lebrun, F., Beck, J.T., Ito, Y., Yardley, D., Deleu, I., Perez, A., Bachelot, T., Vittori, L., Xu, Z., Mukhopadhyay, P., Lebwohl, D., Hortobagyi, G.N., 2012. Everolimus in postmenopausal hormone-receptor-positive advanced breast cancer. N. Engl. J. Med. 366, 520–529.

Biswas, S.K., Mantovani, A., 2010. Macrophage plasticity and interaction with lymphocyte subsets: cancer as a paradigm. Nat. Immunol. 11, 889–896.

Byles, V., Covarrubias, A.J., Ben-Sahra, I., Lamming, D.W., Sabatini, D.M., Manning, B.D., Horng, T., 2013. The TSC-mTOR pathway regulates macrophage polarization. Nat. Commun. 4, 2834.

Carracedo, A., Ma, L., Teruya-Feldstein, J., Rojo, F., Salmena, L., Alimonti, A., Egia, A., Sasaki, A.T., Thomas, G., Kozma, S.C., Papa, A., Nardella, C., Cantley, L.C., Baselga, J., Pandolfi, P.P., 2008. Inhibition of mTORC1 leads to MAPK pathway activation through a PI3K-dependent feedback loop in human cancer. J. Clin. Invest. 118, 3065–3074.

Chi, H., 2012. Regulation and function of mTOR signalling in T cell fate decisions. Nat. Rev. Immunol. 12, 325–338.

Curran, M.P., 2012. Everolimus: in patients with subependymal giant cell astrocytoma associated with tuberous sclerosis complex. Paediatr. Drugs 14, 51–60.

Dorris 3rd, J.R., Jones, S., 2014. Everolimus in breast cancer: the role of the pharmacist. Ann. Pharmacother. 48, 1194–1201.

Gordon, S., 2003. Alternative activation of macrophages. Nat. Rev. Immunol. 3, 23–35.

Hartung, H.P., Schafer, B., Heininger, K., Stoll, G., Toyka, K.V., 1988. The role of macrophages and eicosanoids in the pathogenesis of experimental allergic neuritis. Serial clinical, electrophysiological, biochemical and morphological observations. Brain 111 (Pt 5), 1039–1059.

Hennig, M., Bauer, D., Wasmuth, S., Busch, M., Walscheid, K., Thanos, S., Heiligenhaus, A., 2012. Everolimus improves experimental autoimmune uveoretinitis. Exp. Eye Res. 105, 43–52.

Hughes, R.A., Cornblath, D.R., 2005. Guillain-Barre syndrome. Lancet 366, 1653–1666.

Hughes, R.A., Swan, A.V., Raphael, J.C., Annane, D., van Koningsveld, R., van Doorn, P.A., 2007. Immunotherapy for Guillain-Barre syndrome: a systematic review. Brain 130, 2245–2257.

Jiang, W., St-Pierre, S., Roy, P., Morley, B.J., Hao, J., Simard, A.R., 2016. Infiltration of CCR2 + Ly6C high proinflammatory monocytes and neutrophils into the central nervous system is modulated by nicotinic acetylcholine receptors in a model of multiple sclerosis. J. Immunol.

Kiefer, R., Kieseier, B.C., Stoll, G., Hartung, H.P., 2001. The role of macrophages in immune-mediated damage to the peripheral nervous system. Prog. Neurobiol. 64, 109–127.

Mantovani, A., Biswas, S.K., Galdiero, M.R., Sica, A., Locati, M., 2013. Macrophage plasticity and polarization in tissue repair and remodelling. J. Pathol. 229, 176–185.

Mercalli, A., Calavita, I., Dugnani, E., Citro, A., Cantarelli, E., Nano, R., Melzi, R., Maffi, P., Secchi, A., Sordi, V., Piemonti, L., 2013. Rapamycin unbalances the polarization of human macrophages to M1. Immunology 140, 179–190.

Mosser, D.M., Edwards, J.P., 2008. Exploring the full spectrum of macrophage activation. Nat. Rev. Immunol. 8, 958–969.

O'Reilly, K.E., Rojo, F., She, Q.B., Solit, D., Mills, G.B., Smith, D., Lane, H., Hofmann, F., Hicklin, D.J., Ludwig, D.L., Baselga, J., Rosen, N., 2006. mTOR inhibition induces upstream receptor tyrosine kinase signaling and activates Akt. Cancer Res. 66, 1500–1508.

Pereira-Lopes, O., Sampaio-Maia, B., Sampaio, S., Vieira-Marques, P., Monteiro-da-Silva, F., Braga, A.C., Felino, A., Pestana, M., 2013. Periodontal inflammation in renal transplant recipients receiving everolimus or tacrolimus - preliminary results. Oral Dis. 19, 666–672.

Saran, U., Foti, M., Dufour, J.F., 2015. Cellular and molecular effects of the mTOR inhibitor everolimus. Clin. Sci. 129, 895–914.

Sarkey, J.P., Richards, M.P., Stubbs Jr., E.B., 2007. Lovastatin attenuates nerve injury in an animal model of Guillain-Barre syndrome. J. Neurochem. 100, 1265–1277.

Shi, Y., Yan, H., Frost, P., Gera, J., Lichtenstein, A., 2005. Mammalian target of rapamycin inhibitors activate the AKT kinase in multiple myeloma cells by up-regulating the insulin-like growth factor receptor/insulin receptor substrate-1/phosphatidylinositol 3-kinase cascade. Mol. Cancer Ther. 4, 1533–1540.

Sica, A., Mantovani, A., 2012. Macrophage plasticity and polarization: in vivo veritas. J. Clin. Invest. 122, 787–795.

Song, M.S., Salmena, L., Pandolfi, P.P., 2012. The functions and regulation of the PTEN tumour suppressor. Nat. Rev. Mol. Cell Biol. 13, 283–296.

Su, X., Yu, Y., Zhong, Y., Giannopoulou, E.G., Hu, X., Liu, H., Cross, J.R., Ratsch, G., Rice, C.M., Ivashkiv, L.B., 2015. Interferon-gamma regulates cellular metabolism and mRNA translation to potentiate macrophage activation. Nat. Immunol. 16, 838–849.

Vitiello, D., Neagoe, P.E., Sirois, M.G., White, M., 2015. Effect of everolimus on the immunomodulation of the human neutrophil inflammatory response and activation. Cell. Mol. Immunol. 12, 40–52.

Wang, G., Shi, Y., Jiang, X., Leak, R.K., Hu, X., Wu, Y., Pu, H., Li, W.W., Tang, B., Wang, Y., Gao, Y., Zheng, P., Bennett, M.V., Chen, J., 2015. HDAC inhibition prevents white matter injury by modulating microglia/macrophage polarization through the GSK3beta/PTEN/Akt axis. Proc. Natl. Acad. Sci. U. S. A. 112, 2853–2858.

Wynn, T.A., Chawla, A., Pollard, J.W., 2013. Macrophage biology in development, homeostasis and disease. Nature 496, 445–455.

Xiao, J., Zhai, H., Yao, Y., Wang, C., Jiang, W., Zhang, C., Simard, A.R., Zhang, R., Hao, J., 2014. Chrysin attenuates experimental autoimmune neuritis by suppressing immuno-inflammatory responses. Neuroscience 262, 156–164.

Xie, L., Sun, F., Wang, J., Mao, X., Xie, L., Yang, S.H., Su, D.M., Simpkins, J.W., Greenberg, D.A., Jin, K., 2014. mTOR signaling inhibition modulates macrophage/microglia-mediated neuroinflammation and secondary injury via regulatory T cells after focal ischemia. J. Immunol. 192, 6009–6019.

Yim, K.L., 2012. Everolimus and mTOR inhibition in pancreatic neuroendocrine tumors. Cancer Manag. Res. 4, 207–214.

Ytting, H., Larsen, F.S., 2015. Everolimus treatment for patients with autoimmune hepatitis and poor response to standard therapy and drug alternatives in use. Scand. J. Gastroenterol. 50, 1025–1031.

Yuki, N., Hartung, H.P., 2012. Guillain-Barre syndrome. N. Engl. J. Med. 366, 2294–2304.

Zhang, Z., Zhang, Z.Y., Schluesener, H.J., 2009. Compound A, a plant origin ligand of glucocorticoid receptors, increases regulatory T cells and M2 macrophages to attenuate experimental autoimmune neuritis with reduced side effects. J. Immunol. 183, 3081–3091.

Zhang, H.L., Hassan, M.Y., Zheng, X.Y., Azimullah, S., Quezada, H.C., Amir, N., Elwasila, M., Mix, E., Adem, A., Zhu, J., 2012. Attenuated EAN in TNF-alpha deficient mice is associated with an altered balance of M1/M2 macrophages. PLoS One 7, e38157.

Zhang, H.L., Zheng, X.Y., Zhu, J., 2013. Th1/Th2/Th17/Treg cytokines in Guillain-Barre syndrome and experimental autoimmune neuritis. Cytokine Growth Factor Rev. 24, 443–453.

Zhang, C.J., Zhai, H., Yan, Y., Hao, J., Li, M.S., Jin, W.N., Su, N., Vollmer, T.L., Shi, F.D., 2014. Glatiramer acetate ameliorates experimental autoimmune neuritis. Immunol. Cell Biol. 92, 164–169.

Zhu, J., Mix, E., Link, H., 1998. Cytokine production and the pathogenesis of experimental autoimmune neuritis and Guillain-Barre syndrome. J. Neuroimmunol. 84, 40–52.